Absence of Spin Liquid Behavior in Nd$_3$Ga$_5$SiO$_{14}$ Using Magneto-Optical Spectroscopy

X. S. Xu,[1] T. V. Brinzari,[1] S. McGill,[2] H. D. Zhou,[2] C. R. Wiebe,[2,3] and J. L. Musfeldt[1]

[1]*Department of Chemistry, University of Tennessee, Knoxville, Tennessee 37996, USA*
[2]*National High Magnetic Field Laboratory, Tallahassee, Florida 32310, USA*
[3]*Department of Physics, Florida State University, Tallahassee, Florida 32306, USA*
(Received 12 July 2009; published 23 December 2009)

We measured the low-lying crystal field levels of Nd^{3+} in Nd$_3$Ga$_5$SiO$_{14}$ via magneto-optical spectroscopy and employed the extracted energies, magnetic moments, and symmetries to analyze the magnetic properties and test the spin liquid candidacy of this material. The exchange interaction is surprisingly small, a discovery that places severe constraints on models used to describe the ground state of this system. Further, it demonstrates the value of local-probe photophysical techniques for rare-earth-containing materials where bulk property measurements can be skewed by low-lying electronic structure.

A spin liquid is an intriguing state of matter in which frustration prevents spin order due to significant exchange interactions [1]. It was proposed many years ago by Anderson [2] but has been challenging to realize [3,4]. To show that a material is a physical manifestation of a spin liquid, one has to demonstrate that the system does not order even at very low temperature and that exchange interactions are strong. The recently discovered rare earth Langasites are promising spin liquid candidates because they display cooperative paramagnetic behavior and no long-range ordering down to 35 mK [5–9]. It remains to test whether exchange interactions between the rare earth centers in Nd$_3$Ga$_5$SiO$_{14}$ are significant. This is challenging because low-lying crystal field levels can complicate the magnetization [10]. Our approach is different in that we exploit Nd^{3+} as a local probe of low-lying electronic structure and magnetism [11–16] and use this data to assess the second key requirement for a spin liquid state. Surprisingly, we find that exchange interactions are weak, demonstrating that this system is an isolated spin paramagnet rather than a spin liquid.

The crystal structure of Nd$_3$Ga$_5$SiO$_{14}$ displays a distorted kagome lattice of Nd^{3+} ions arranged in the *ab* plane. Here, Nd^{3+} occupies a site of local C_2 symmetry, at the center of a square antiprism and connected to eight oxygen atoms [Fig. 1(a)]. Neutron scattering and muon spin relaxation indicate no order down to 35 mK [7,9]. At the same time, magnetization yields a Curie-Weiss temperature of −52 K (or −62 K) and a Curie-Weiss moment of 3.5μ_B (or 3.8μ_B) [5,7]. Taken together, these data point toward a large frustration factor (>1300) that naively signals strong interactions [5–7]. A low temperature saturation magnetization of 1.5μ_B per Nd^{3+} is also observed [5,7]. The ground state multiplet of Nd^{3+} in free space is $^4I_{9/2}$, with a tenfold degeneracy due to strong spin-orbit coupling. The aforementioned local environment [Fig. 1(a)] gives rise to a magnetocrystalline anisotropy. Thus, for Nd^{3+} in Nd$_3$Ga$_5$SiO$_{14}$, the $^4I_{9/2}$ multiplet splits into several levels, each with a different magnetic moment.

These low-lying crystal field levels contribute to the magnetic response. This issue was recently investigated by Simonet *et al.* [8], although incomplete information on the crystal field energies and their independent magnetic moments precluded a full analysis.

In this Letter, we focus on the photo-physics of Nd$_3$Ga$_5$SiO$_{14}$, advantageously combining local probe and high magnetic field techniques to elucidate the low-lying electronic structure, bulk magnetic properties, and exchange interaction, the latter of which, if strong, would constitute an important signature of the elusive spin liquid state. Instead, we find that the bulk magnetic properties can be quantitatively explained assuming isolated Nd^{3+} sites and that the exchange interaction, critical for testing spin liquid character, is small (≤ 0.01 meV). This result rules out Nd$_3$Ga$_5$SiO$_{14}$ as a spin liquid, at least down to 100 mK.
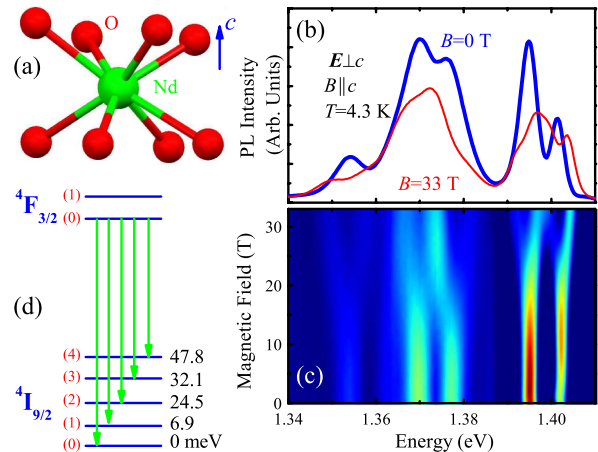

FIG. 1 (color online). (a) Local square antiprismatic environment of the Nd^{3+} centers. (b) PL spectra at 4.3 K. (c) Magnetic field dependence of the PL at 4.3 K for $\vec{B} \parallel c$. Gray scale (color) denotes intensity: dark (blue) is low; bright (red) is high. (d) Energy level diagram of the $^4F_{3/2} \rightarrow {}^4I_{9/2}$ emission, with crystal field splitting extracted from the peak positions in (b).

Large single crystals with both $(001)_{hex}$ and $(100)_{hex}$ faces were grown by floating-zone techniques [7,17]. Transmittance was carried out using a series of spectrometers (3 meV–6 eV). The absorption coefficient was calculated directly from the transmittance. Photo-luminescence (PL) was measured using the 750 nm excitation from a Ti-sapphire laser. Both sets of spectra were collected between 4.3–300 K and 0–33 T. PL lifetime studies employed lock-in techniques and were performed at 4.3 K in magnetic fields up to 17.5 T.

The magnetic properties of $Nd_3Ga_5SiO_{14}$ arise from $4f$ electrons in the Nd^{3+} centers and their interaction in the solid state, making an understanding of their energetics key to our investigation. For transparent materials, PL is an incisive technique for determining the f manifold electronic energy levels [18]. In Nd^{3+}-containing materials, it is well known that radiative emission from the metastable $^4F_{3/2}$ level is strong [12]. In our experiment, we observed three PL groups centered at ≈ 1.37, 1.14, and 0.90 eV. They can be assigned as $^4F_{3/2} \rightarrow ^4I_{9/2}$, $^4F_{3/2} \rightarrow ^4I_{11/2}$, and $^4F_{3/2} \rightarrow ^4I_{13/2}$ transitions, respectively [12]. Here, we focus on the $^4F_{3/2} \rightarrow ^4I_{9/2}$ cluster because the $^4I_{9/2}$ multiplet contains the ground state levels which are most important for evaluating the magnetic properties. As shown in Figs. 1(b) and 1(c), the $^4F_{3/2} \rightarrow ^4I_{9/2}$ cluster shows rich fine structure. At zero magnetic field, five peaks can be identified. These features arise due to lifting of spatial degeneracy in $^4I_{9/2}$, yielding five low-lying crystal field levels and a remaining Kramers' degeneracy [Fig. 1(d)]. We assign the peaks in Figs. 1(b) and 1(c) to the energy levels of the $^4I_{9/2}$ multiplet [19] and extract the energy separation between crystal field levels from the peak positions. The results are shown schematically in Fig. 1(d) and summarized in Table I.

To complement our experimental work, we also carried out a group theoretical analysis of the crystal field splitting using the point charge model. Although the formal site symmetry of Nd^{3+} in the square antiprismatic environment is C_2, we employed D_4 to a good approximation. Since the $^4I_{9/2}$ multiplet has a half-integer total angular momentum quantum number, we used the double group D'_4 [20], for

TABLE I. Summary of the low-lying crystal field levels of Nd^{3+} in $Nd_3Ga_5SiO_{14}$, their symmetries, and the magnetic properties of the $^4I_{9/2}$ multiplet. The energies and magnetic moments are extracted from the peak positions and their field dependence of the PL spectra, as shown in Figs. 1(b) and 1(c).

State	E (meV)	E_{fit} (meV)	IR [a]	μ (μ_B)
$^4I_{9/2}(4)$	47.8	48.2	Γ_6	2.59
$^4I_{9/2}(3)$	32.1	31.1	Γ_6	1.77
$^4I_{9/2}(2)$	24.5	24.4	Γ_7	2.45
$^4I_{9/2}(1)$	6.9	6.8	Γ_6	1.40
$^4I_{9/2}(0)$	0	0	Γ_7	1.32

[a]IR stands for irreducible representation.

which the representation of $^4I_{9/2}$ can be reduced to the set of $3\Gamma_6 + 2\Gamma_7$ irreducible representations, corresponding to the 5 possible energy levels [21]. Employing the point charge model, we fit the zero field and 33 T PL spectra with the spin Hamiltonian $\mathcal{H} = A_2^0O_2^0 + A_4^0O_4^0 + A_4^4O_4^4 + A_6^0O_6^0 + A_6^4O_6^4 - g\mu_B\vec{J}\cdot\vec{B}$, where O_k^q are angular momentum operators whose expressions are given in Ref. [22], A_k^q are fitting parameters, $g = 8/11$ is the Landé g factor for $^4I_{9/2}$, $\vec{J}$ is the total angular moment quanta, and $\vec{B}$ is the magnetic field [23]. The energy levels obtained from this fit are summarized in Table I. The assignment of specific irreducible representations to the crystal field levels is done from an analysis of the associated wave functions [21].

We can use this data to extract and analyze the magnetic properties of the crystal field levels in the $^4I_{9/2}$ multiplet. From Fig. 1(c), one can see that the 5 characteristic peaks of the zero field emission spectrum split into 10 in applied magnetic field ($\vec{B} \parallel c$). This splitting is due to the Zeeman effect. In contrast, when $\vec{B} \perp c$, peak shifts are relatively modest (data not shown), confirming that the low temperature easy axis is along c [5]. In principle, the observed peak shifts and splittings in the emission spectrum for $\vec{B} \parallel c$ are due to a combination of Zeeman effects from both the $^4I_{9/2}$ and $^4F_{3/2}$ levels. We therefore begin by considering the contribution from $^4F_{3/2}$. Group theory predicts that $^4F_{3/2}$ splits into two energy levels in D'_4 symmetry: $^4F_{3/2}(0) = |J = \frac{3}{2}, J_z = \frac{1}{2}\rangle \pm |J = \frac{3}{2}, J_z = -\frac{1}{2}\rangle$ and $^4F_{3/2}(1) = |J = \frac{3}{2}, J_z = \frac{3}{2}\rangle \pm |J = \frac{3}{2}, J_z = -\frac{3}{2}\rangle$. These states correspond to irreducible representations Γ_6 and Γ_7, respectively. Using the parameters found in the analysis of the $^4I_{9/2}$ levels [23], one finds that $^4F_{3/2}(0)$ is the lower energy state. It contributes an energy shift of $\delta E = g\mu_B B B_r^{1/2}(x)$. Here, $g = 0.2$ for $^4F_{3/2}$, $B_r^{1/2}(x)$ is the Brillouin function [24] with $x \equiv \frac{g\mu_B B}{2k_B T}$, and k_B and T are Boltzmann constant and temperature, respectively. For example, at $T = 4.3$ K and $B = 33$ T, $\delta E/B = 0.155\mu_B$. Taking this contribution into account, we extracted magnetic moments $\mu \equiv |dE/dB|$ for each energy level in the $^4I_{9/2}$ multiplet. These moments are summarized in Table I. We find that each crystal field level has a different magnetic moment and, in general, moment size increases with energy.

Direct transmittance experiments provide additional information on the magnetic properties of the Nd^{3+} $4f$ electrons. Figure 2(a) displays the 10 K transmittance spectrum between 1.3 and 2.5 eV. It shows the well-known Nd^{3+} absorption features [12], with fine structure arising from the crystal field. Figure 2(b) shows a schematic energy diagram of the $^4I_{9/2} \rightarrow ^4F_{3/2}$ excitation. Because only the $^4I_{9/2}(0)$ level is populated at low temperature, we assign the two features in Fig. 2(c) as $^4I_{9/2}(0) \rightarrow ^4F_{3/2}(0)$ and $^4I_{9/2}(0) \rightarrow ^4F_{3/2}(1)$ excitations. As shown in Fig. 2(c),

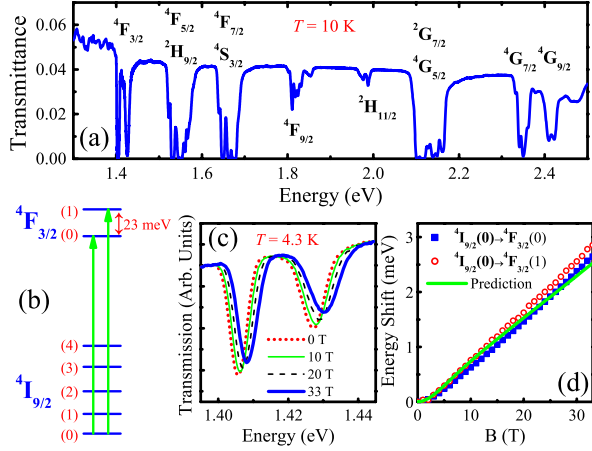FIG. 2 (color online). (a) 10 K transmittance spectrum where features correspond to excitations from the $^4I_{9/2}$ ground state to higher energy multiplets, as indicated. (b) Schematic energy diagram of the excitations observed between 1.40 and 1.45 eV. (c) Close-up view of the data for $B = 0$, 10, 20, and 33 T which probes the indicated $^4I_{9/2} \rightarrow \,^4F_{3/2}$ excitations. (d) Comparison of the measured shift in the two $^4I_{9/2} \rightarrow \,^4F_{3/2}$ excitations with that predicted using the magnetic moment extracted from our complementary PL experiments (Table I).

the transmittance minima shift toward higher energy with increasing field. Assuming that the energy shift comes from Zeeman splitting of the $^4I_{9/2}(0)$ level, one has $\delta E = \mu B \tanh(\frac{\mu B}{k_B T})$. Using $\mu = 1.32\mu_B$ from the PL experiments and $T = 4.3$ K, the relation between δE and magnetic field B is plotted in Fig. 2(d), in excellent agreement with the observed energy shift of the $^4I_{9/2}(0) \rightarrow \,^4F_{3/2}(0)$ and $^4I_{9/2}(0) \rightarrow \,^4F_{3/2}(1)$ excitations. The discrepancy at high field may come from mixing between $^4I_{9/2}(0)$ and higher energy $^4I_{9/2}$ states. The field-induced broadenings in the $^4I_{9/2}(0) \rightarrow \,^4F_{3/2}(0)$ and $^4I_{9/2}(0) \rightarrow \,^4F_{3/2}(1)$ excitations are in line with the wave functions discussed above.

Knowledge of the energies and magnetic moments of the low-lying crystal field levels allows us to quantitatively understand the magnetic properties of $Nd_3Ga_5SiO_{14}$. A key assumption is isolated Nd^{3+} sites. When site-to-site interaction is weak, the average magnetic moment of an ensemble of Nd^{3+} centers can be written as $\langle\mu\rangle = \sum_i \sum_{\sigma=-1,1} \mu_i e^{-(\sigma\mu_i B + E_i)/k_B T} / \sum_i \sum_{\sigma=-1,1} e^{-(\sigma\mu_i B + E_i)/k_B T}$, where μ_i and E_i are magnetic moment and energy of the $^4I_{9/2}(i)$ levels, respectively. In the low temperature or high magnetic field limit, $\langle\mu\rangle = \mu_0 = 1.32\mu_B$, which is the moment of the $^4I_{9/2}(0)$ level, in good agreement with the $1.5\mu_B$ per Nd^{3+} saturation magnetization at low temperature [5,7]. At high temperature,

$$\langle\mu\rangle = \frac{\sum_i \mu_i^2 B/N}{k_B T + \sum_i \mu_i^2 E_i / \sum_i \mu_i^2 - \sum_i E_i}, \quad (1)$$

where $N = 5$ is the number of $^4I_{9/2}$ levels. Defining $C \equiv$

$\sum_i \mu_i^2/k_B N$, and $-\theta \equiv (\sum_i \mu_i^2 E_i / \sum_i \mu_i^2 - \sum_i E_i)/k_B$, Eq. (1) becomes the Curie-Weiss law: $\langle\mu\rangle = \frac{CB}{T-\theta}$, where θ is the Curie-Weiss temperature. Using the data in Table I, we find $\theta = -87$ K, close to that obtained from magnetization (-52 and -62 K) [5,7]. The small discrepancy may come from the fact that optical excitations sample all $^4I_{9/2}$ levels. In addition, one can calculate the Curie-Weiss moment $\mu_{CW} \equiv \sqrt{3k_B C} = 3.4\mu_B$, in good agreement with that obtained from magnetization (3.8 and $3.5\mu_B$) [5,7]. We conclude that the apparent Curie-Weiss law in $Nd_3Ga_5SiO_{14}$ is a consequence of thermal activation of Nd^{3+} crystal field levels with higher magnetic moments. It is not due to a thermal fluctuation-induced reduction in spin antialignment [10].

Although consideration of the crystal field energies and the individual magnetic moments of these states explains the magnetization, interactions between Nd^{3+} sites may still be present [8]. Evaluating the magnitude of exchange interactions in rare earth-containing systems is challenging because magnetization is a bulk technique that is difficult to interpret when spin-spin interactions arising from f manifold crystal field excitations interfere [10]. In principle, significant exchange interactions may lift the Kramers' degeneracy in each $^4I_{9/2}$ multiplet, causing further splitting in the spectra. Although this information can not be directly extracted from absorption and emission spectra due to finite line width effects, we can estimate the energy scale of the exchange interaction from combined PL lifetime data and an extended analysis of the absorption spectrum.

Figure 3(a) displays the PL decay profile. The characteristic time scale is on the order of 10 μs, which is relatively long. The emission involves both radiative and nonradiative decay processes. We can estimate the intrinsic radiative decay rate directly from the low temperature absorption spectrum [Fig. 3(b)]. Using the partial sum rule, we calculate the oscillator strength of the $^4I_{9/2} \rightarrow \,^4F_{3/2}$ excitation as $f \equiv \frac{2c}{\hbar\pi\omega_p^2} \int_{E_1}^{E_2} n\alpha dE = 5.9 \times 10^{-6}$.
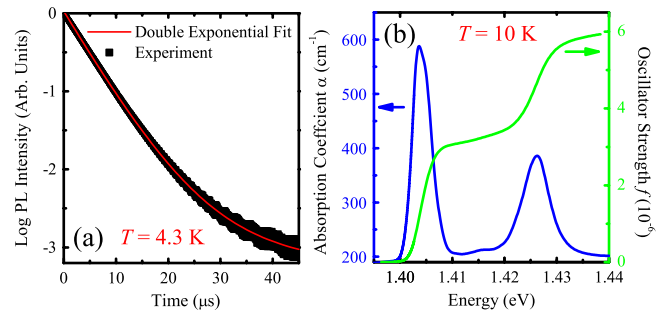

FIG. 3 (color online). (a) PL intensity vs time from which we extract lifetime information. The experimental data are fit with a double exponential function $I = I_1 e^{-t/\tau_1} + I_2 e^{-t/\tau_2}$ setting $\tau_2 = 100$ μs. τ_1 is found to be 8.7 μs. The life time decreases by $\leq 5\%$ at 17.5 T. (b) Close-up absorption and oscillator strength corresponding to the two $^4I_{9/2} \rightarrow \,^4F_{3/2}$ excitations, from which we estimate the radiative decay rate.

Here, α is the absorption coefficient, $n \approx 2$ is the refractive index, ω_p is the plasma frequency $\equiv \sqrt{\frac{e^2 \rho}{m \epsilon_0}}$, ρ is the number density of Nd sites, c is the speed of light, e and m are the charge and mass of an electron, ϵ_0 is the vacuum dielectric constant, and E_1 and E_2 are the energies of integration [25]. According to Judd-Ofelt theory [13], the radiative decay rate can be evaluated as $A = \frac{\omega^2 e^2 n^2}{2mc^3 \pi \epsilon_0} f \approx 2.8 \times 10^3 \text{ s}^{-1}$, where ω is the angular frequency corresponding to the $^4F_{3/2} \rightarrow {}^4I_{9/2}$ transition. Considering the other decay processes (e.g., $^4F_{3/2} \rightarrow {}^4I_{11/2}$ and $^4F_{3/2} \rightarrow {}^4I_{13/2}$), we estimate that the total radiative decay rate is on the order of $1 \times 10^4 \text{ s}^{-1}$ [13]. This corresponds to a 100 μs life time, consistent with typical lifetimes of other materials containing diluted Nd^{3+} centers [14] but longer than that observed in $Nd_3Ga_5SiO_{14}$ [Fig. 3(a)]. The factor of 10 degradation in the real system compared to the intrinsically expected value suggests an important role for nonradiative decay mechanisms, which typically involves interaction between Nd^{3+} sites [26]. As shown in Fig. 3(a), a double exponential decay function fits the experimental data very well [13–15]. This points toward dominant long-range dipole-dipole interactions rather than short-range exchange interactions since the latter should display faster-than-exponential decay [13–15,27]. One can extract an order of magnitude estimate of the dipole-dipole interaction energy between Nd^{3+} sites as $W = \frac{p^2}{4\pi\epsilon_0 R^3} \sim 0.01$ meV [28]. Here, $R = 4.2$ Å is the nearest distance between Nd^{3+} sites, $p \sim 1 \times 10^{-31}$ C $\cdot$ m is the electric dipole moment of Nd^{3+} estimated according to Ref. [16], and ϵ_0 is the vacuum permittivity. The exchange interaction, which appears to be weaker than the dipole-dipole interaction, should therefore have a smaller energy scale. Our ongoing mean-field analysis of existing magnetization data [6] supports a similarly small energy scale [29]. Neutron scattering and heat capacity experiments reveal an activated barrier-doublet splitting of ≈ 0.02 meV, consistent with our results [7,8].

In summary, we employed high field photo-physical techniques to elucidate the low-lying electronic structure, bulk magnetic properties, and exchange interactions of the candidate spin liquid material $Nd_3Ga_5SiO_{14}$. The unexpectedly small exchange interaction leads to a revised frustration factor of ~ 1 and rules out $Nd_3Ga_5SiO_{14}$ as a spin liquid, at least down to 100 mK. On the other hand, Nd^{3+} is widely recognized as one of the most efficient rare earth ions for solid-state and up conversion lasers [12–15], so the weak interaction makes $Nd_3Ga_5SiO_{14}$ a promising optical material. This work demonstrates the power and breadth of magneto-optical spectroscopy, positioning it to advance magnetic property determination in other frustrated, multiferroic, and superconducting rare-earth-containing oxides.

[1] B. G. Levi, Phys. Today **60**, No. 2, 16 (2007).
[2] P. W. Anderson, Mater. Res. Bull. **8**, 153 (1973).
[3] A. P. Ramirez, in *Handbook of Magnetic Materials*, edited by K. H. J. Buschow (Elsevier, New York, 2001), Vol. 13.
[4] S. T. Bramwell, and M. J. P. Gingras, Science **294**, 1495 (2001).
[5] P. Bordet *et al.*, J. Phys. Condens. Matter **18**, 5147 (2006).
[6] J. Robert *et al.*, Phys. Rev. Lett. **96**, 197205 (2006).
[7] H. D. Zhou *et al.*, Phys. Rev. Lett. **99**, 236401 (2007).
[8] V. Simonet *et al.*, Phys. Rev. Lett. **100**, 237204 (2008).
[9] A. Zorko *et al.*, Phys. Rev. Lett. **101**, 026405 (2008).
[10] L. Beaury *et al.*, J. Phys. Condens. Matter **6**, 5169 (1994).
[11] H. M. Crosswhite and H. W. Moos, *Optical Properties of Ions in Crystals* (Interscience, New York, 1967).
[12] R. Balda *et al.*, Phys. Rev. B **64**, 144101 (2001).
[13] G. A. Kumar, A. Martinez, and E. De La Rosa, J. Lumin. **99**, 141 (2002).
[14] V. Ostroumov *et al.*, J. Opt. Soc. Am. B **15**, 1052 (1998).
[15] V. Lupei *et al.*, J. Appl. Phys. **66**, 3792 (1989).
[16] W. M. Yen *et al.*, Phys. Rev. **140**, A1188 (1965).
[17] The sample thickness was 0.17 mm.
[18] D. J. Newman, and B. Ng, *Crystal Field Handbook* (Cambridge University Press, Cambridge, UK, 2000).
[19] Fine structure in the $^4F_{3/2}$ state may introduce complexity into the $^4F_{3/2} \rightarrow {}^4I_{9/2}$ transition. The fact that $^4F_{3/2}$ is split into two levels with 23 meV separation (see transmittance spectra) suggests that only the lower level of the $^4F_{3/2}$ multiplet participates in the transition at 4 K.
[20] F. A. Cotton, *Chemical Applications of Group Theory* (Interscience, New York, 1967).
[21] K. R. Lea, M. J. M. Leask, and W. P. Wolf, J. Phys. Chem. Solids **23**, 1381 (1962).
[22] J. M. Baker, B. Bleaney, and W. Hayes, Proc. R. Soc. A **247**, 141 (1958).
[23] $A_2^0 = 0.196$ meV, $\quad A_4^0 = 0.528$ meV, $\quad A_4^4 = 2.64$ meV, $A_6^0 = -0.148$ meV, and $A_6^4 = 1.10$ meV.
[24] C. Kittel, *Introduction to Solid State Physics* (Wiley, New York, 2005).
[25] F. Wooten, *Optical Properties of Solids* (Academic Press, New York, 1972).
[26] D. L. Dexter, and J. H. Schulman, J. Chem. Phys. **22**, 1063 (1954).
[27] Because of their long-range interactions, classical dipole interactions yield an exponential decay (with a constant decay rate). On the other hand, for shorter range exchange interactions, the decay rate is sensitive to the concentration of excited Nd^{3+} centers. This is because only near neighbors interact, and it results in a rapidly decreasing (faster-than-exponential) decay rate.
[28] J. D. Jackson, *Classical Electrodynamics* (Wiley, New York, 1962).
[29] X. S. Xu *et al.*, unpublished results.